Simulated radiative forcing from contrails and contrail cirrus

Chih-Chieh Chen and Andrew Gettelman

National Center for Atmospheric Research, P.O. Box 3000, Boulder CO 80307-3000, USA

Correspondence to: Chih-Chieh Chen, cchen@ucar.edu

Abstract. A comprehensive general circulation model including ice supersaturation is used to estimate the climate impact of aviation induced contrails. The model uses a realistic aviation emissions inventory for 2006 to initiate contrails, and allows them to evolve consistently with the model hydrologic cycle.

The radiative forcing from linear contrails is very sensitive to the diurnal cycle. For linear contrails, including the diurnal cycle of air traffic reduces the estimated radiative forcing by 29%, and for contrail cirrus estimates, the radiative forcing is reduced by 25%. Estimated global radiative forcing from linear contrails is $0.0031\pm0.0005\,\mathrm{Wm}^{-2}$. The linear contrail radiative forcing is found to exhibit a strong diurnal cycle. The contrail cirrus radiative forcing is less sensitive to the diurnal cycle of flights. The estimated global radiative forcing from contrail cirrus is $0.012\pm0.01\,\mathrm{Wm}^{-2}$. Over regions with the highest air traffic, the regional effect can be as large as 1 Wm^{-2}.

Keywords. contrail, climate modeling, radiative forcing, aviation impact

1 Introduction

Aircraft effects on clouds, have significant impacts on climate (Lee et al., 2010; Burkhardt et al., 2010). When aircraft exhaust mixes with ambient air, liquid drops may form and freeze if the ambient air is cold and the humidity is high (Schmidt, 1941; Appleman, 1953), forming 'condensation trails' or contrails, behind an aircraft. These line-shaped cirrus, the so-called linear contrails, may persist and take up water vapor from ambient air if the air is supersaturated with respect to ice. Persistent contrails may last minutes up to several hours (Minnis et al., 1998). Additional cloudiness beyond line-shaped contrails may be induced due to the spreading and shearing of contrails, known as contrail cirrus (Schumann and Wendling, 1990; Minnis et al., 1998).

Like natural cirrus, contrails have a radiative forcing effect on climate (Marquart and Mayer, 2002), cooling in the shortwave by reflecting radiation to space, but heating in the longwave due to a low emission temperature. The longwave effect is thought to dominate for these clouds in the long-term average (Dietmüller et al. , 2008; Rap et al., 2010). Estimates of radiative forcing associated with linear contrails range from 2 to 10 miliwatts per square meter (mWm^{-2}) (see summary in Lee et al., 2010). The uncertainty mainly results from the coverage and optical depth of contrails (Lee et al., 2010). Some studies (Myhre and Stordal, 2001; Stuber and Forster, 2006, 2007; Fromming et al. , 2011; Newinger and Burkhardt, 2012) showed that the diurnal cycle of air traffic can also affect contrail radiative forcing. Stuber and Forster (2007) found that 60% of the global mean contrail radiative forcing was attributed to night flights even though they only accounted for 40% of the distance travelled by aircraft, and Newinger and Burkhardt (2012) reported 54% and 63% of the net contrail radiative forcing over the US and Western Europe, respectively, was due to night flights.

Uncertainties in assessing the radiative forcing due to contrail cirrus are even higher. It is routinely observed that line-shape contrails subsequently shear and spread after formation, termed contrail cirrus, and the additional cloudiness due to spreading may increase by a factor of 1.8 (Minnis et al., 2004). Larger spreading factors were reported by a recent study by Burkhardt and Kärcher (2011) in which they found an estimated radiative forcing of 31 mWm^{-2} for contrail cirrus by numerical simulations of a general circulation model (GCM) using a separate contrail cloud class.

In this study, the radiative forcing of linear contrails and contrail cirrus is assessed by using the Community Atmosphere Model Version 5 (CAM5), of the National Center for Atmospheric Research (NCAR) Community Earth System Model (CESM). We employ an integrated approach to contrails by treating them as part of the model hydrologic cycle. This is possible because CAM5 now includes ice supersaturation and can simulate the key formulation and evolution

process of contrails. A detailed aviation emissions inventory is incorporated into CAM5 and the importance of the consideration of the daily cycle of flights is examined by using aircraft emissions averaged on an hourly, daily, and monthly basis. The model and experimental design are described in Section 2, results are presented in Section 3, and discussions are in Section 4.

2 Methodology

2.1 Model description

This work uses CAM version 5 (Gettelman et al., 2010; Neale et al., 2010). The model includes a detailed treatment of cloud liquid and ice microphysics (Morrison and Gettelman, 2008), including a representation of particle size distributions, a detailed mixed phase with a representation of water uptake onto ice (the Bergeron-Findeisen process) and ice supersaturation (Gettelman et al., 2010). This is coupled to a consistent radiative treatment of ice clouds, and an aerosol model that includes particle effects on liquid and ice clouds (Liu et al., 2012). Critical for contrail formation, CAM5 can simulate the mean relative humidity and reproduce the distribution of the frequency of ice supersaturation in the upper troposphere and lower stratosphere (UTLS) (Chen et al., 2012) as observed from the Atmospheric Infra Red Sounder (AIRS) satellite (Gettelman et al., 2006), including the hemispheric asymmetry of higher frequency of supersaturation at Southern Hemisphere midlatitudes.

2.2 Contrail Parameterization

The contrail parameterization used is described in detail by Chen et al. (2012). The parameterization follows the Schmidt-Appleman Criteria (Schmidt, 1941; Appleman, 1953): persistent contrails form if the ambient air temperature is below a critical temperature (Schumann, 1996), and the relative humidity is above ice supersaturation. When contrails are triggered, ambient water vapor above ice supersaturation in the contrails is added to condensate. The volume of the contrails is a product of the flight path distance and a cross-sectional area, assumed to be 300 m $\times$ 300 m (Chen et al., 2012). Ice particles within the contrails are assumed to be spherical and have an initial diameter of 10 μm (Schröder et al., 2000). The assumption on the particle shape and size has a significant impact on the contrail radiative forcing and will be discussed further in Section 3.2. The enhancement of cloud fraction due to formation of persistent contrails is equal to the contrail ice mass, consisted of the aircraft water vapor emissions and the ambient humidity, divided by an assumed empirical value for the In-Cloud Ice Water Content (ICIWC) (Schumann, 2002). Chen et al. (2012) demonstrated that this contrail parameterization was able to produce a reasonable spatial and seasonal distribution of contrails compared to observations.

Chen et al. (2012) demonstrated that this contrail parameterization is sensitive to the initial ice particle size assumed and the cross-sectional area of contrails. The volume of contrails upon formation determines how much ambient humidity from the supersaturated region is taken into the contrails. These uncertainties were examined in Chen et al. (2012). For example, use of a more moderate ice particle size in contrail initialization will enhance ice number concentration and reflectance. A reduction of the cross-sectional area in contrail initialization will decrease the amount of ice mass in contrails and the contrail coverage. Chen et al. (2012) found a reduction of the cross-sectional area from 300 m $\times$ 300 m to 100 m $\times$ 100 m results in a decrease in ice mass by a factor of 4 and a decrease in contrail coverage by a factor of 2.

2.3 Modeling framework

Previous estimates on the globally-averaged contrail radiative forcing indicated that the magnitude of the forcing associated with linear contrails was less than 10 mWm^{-2} (Lee et al., 2010) and the radiative forcing of contrail cirrus could reach 31 mWm^{-2} (Burkhardt and Kärcher, 2011) based on a comprehensive estimate with a GCM. There are higher estimates in the literature, e.g. (Stordal et al., 2005) estimated aircraft-induced cloudiness based on observed trends in cirrus coverage and reported an estimated radiative forcing between 10 and 80 mWm^{-2}. More recently, Schumann and Graf (2013) reported an estimated contrail radiative forcing of 50 mWm^{-2} (40-80 mWm^{-2}) based on the same global aircraft emissions employed in this study.

Capturing such small perturbations through GCM simulations is a major challenge since the variability of the model may be higher than the contrail forcing. Estimates with a free running CAM5 indicate that the detectable (95% confidence limit for a student's t-test) globally averaged radiative flux perturbation at the top of the atmosphere to distinguish any radiative flux perturbation from the model internal variability is 100 mWm^{-2}, from a 20-year simulation. The radiative forcing due to linear contrails and contrail cirrus is very likely to be lower than 100 mWm^{-2} and thus the free-running mode of CAM5 is not an adequate modeling framework for this study.

The model variability of CAM5 is reduced by driving simulations using specified dynamics (CAM5-SD). Using fixed meteorology (imposed pressure, winds and atmospheric and sea surface temperatures) a globally-averaged perturbation above 10 mWm^{-2} is statistically significant, based on the 95% confidence level of a student's t-test from a 20-year simulation with repeating yearly meteorology (see solid curve in Fig. 1). As aircraft emissions are incorporated into CAM5-SD simulations, globally-averaged radiative fluxes at the top of the atmosphere surpass the model variabilities by the end of 20-year simulations as shown in Fig. 1.

In order to address the meteorological and statistical uncertainties and to gain more confidence in our results, we

employ an ensemble modeling technique with four ensemble members. Four different yearly meteorological fields are used to drive each of the four members under CAM5-SD in which aircraft emissions are included. These four yearly meteorologies are obtained by performing a free-running CAM5 simulation without aircraft emissions for four years. In this study, each of the experiments is repeated four times with the only difference in the background meteorological fields. The spread of the four ensemble members allow us to determine: 1) the uncertainty in our calculation of the globally averaged radiative forcing and 2) the significance of local radiative forcing due to the presence of contrails. It is considered significant when the magnitude of local perturbations exceed two standard deviations of the four ensemble members.

As described previously, larger uncertainties could result from the initial contrail particle size assumed and the cross-sectional area of contrails. In this study, we assume a diameter of 10 μm based on contrails aged for 20-30 minutes (Schröder et al., 2000), and a fairly large cross-sectional area (300 m × 300 m) for water uptake based on plume model experiments (H. W. Wong at Aerodyne Research, personal communication 2012).

First we look at linear contrails. We assume that (1) the lifetime of contrails was equal to the time step of CAM5, 30 minutes, (2) all contrails vanished at the end of each time step, and (3) contrails did not feedback on the model state. Thus, these diagnostic calculations (calling the microphysics and radiation code twice with and without contrails and aviation H_2O) yield an estimate of the radiative forcing for linear contrails at each time step. Results are from four ensemble members of 5-year averages by repeating its own meteorology annually. These experiments provide an exact estimate of the linear contrail perturbation with no uncertainty as in Fig. 1, since we are performing a diagnostic calculation at each time step, not computing differences in pairs of simulations. Furthermore, aircraft emssions and contrails are assumed to have no impact on model states. The forcing obtained from these online diagnostic calculations is defined as the "instantaneous effect" which represents our best estimate for linear contrail radiative forcing.

The second set of experiments is designed to look at contrail cirrus in which aircraft water vapor emissions were incorporated into the hydrologic cycle of the model without any assumption on the lifetime of contrails. Contrail initialization is the same as for linear contrails, but the cloud ice in the model is increased, along with ice number and cloud fraction, and the background water vapor is appropriately decreased. The model hydrologic cycle then operates on the contrail as any other cloud and it can freely evolve, but is undifferentiated from other clouds (in contrast to the separate contrail cloud class of Burkhardt and Kärcher (2011)). Linear contrails, once formed, freely evolve during model simulations, depending on the ambient atmospheric temperature and humidity. These experiments are compared with a control simulation without aircraft emissions and the difference in energy balance at the top of the atmosphere is taken as the radiative forcing due to contrail cirrus. Simulations are run on a $1.9^\circ \times 2.5^\circ$ latitude-longitude grid driven by meteorology obtained from a free-running CAM5 simulation with fixed climatological SSTs repeated annually. Results are from four ensemble member of 20 year average differences between a simulation with contrails and aviation water vapor and a simulation without aviation emissions.

3 Results from CAM5-SD simulations

Three experiments were conducted with the Aviation Environmental Design Tool (AEDT) emission inventory (Barrett et al., 2010) which is converted to hourly, daily, and monthly data following the procedure described in Chen et al. (2012). Four different yearly meteorologies, from a four-year free-running CAM5 simulation, were used, separately, to drive four CAM5-SD ensemble simulations, i.e. each member uses a different one-year meteorology repeatedly. Uncertainty in the contrail radiative forcing was represented by two standard deviations among these realizations.

Both the instantaneous and integrated contrail radiative forcing are examined. For linear contrails the estimates are based on diagnostic calculations over 5 years and for contrail cirrus the estimates are based on differences between two simulations over 20 years.

3.1 *Instantaneous effect of contrails*

For linear contrails, the daily cycle of flights is very important in assessing the radiative effects. As illustrated in Fig. 2a and c, when the daily cycle of flights is considered (hourly emissions), the global contrail ice mass exhibits a much stronger diurnal cycle than when using daily or monthly emissions (Fig. 2a). The peak in global contrail ice mass takes place around noon at local time when using hourly emissions, but in the early morning hours when using daily or monthly emissions. The intensity in longwave radiation forcing is found to follow that of the contrail ice mass (Fig. 2a,c). Graf et al. (2012) reported that a strong diurnal cycle could be identified in aviation induced cirrus cover over the North Atlantic flight corridor with two daily peaks at 6 and 18 UTC which correlate well with air traffic. Over the Eastern US and Central Europe, the ice mass and forcing of linear contrails also exhibit very similar behavior as in the global average.

The highest number of flights are located in the Eastern US and Central Europe with more flights taking place during the daytime over the two continents (Chen et al., 2012). The results illustrated in Fig. 2, with model output at each grid point calibrated to its local time, reveal that the peak of the simulated contrail ice mass takes place around noon at local time over both continents. Therefore, averaging aircraft emissions on a monthly or daily basis, which shifts some

daytime flights to the nighttime, alters the radiative forcing. The longwave (heating) effect remains approximately the same in the diurnal average (as discussed below), but the shortwave effect is reduced because more contrails occur in darkness when the diurnal cycle is averaged out.

Similar results have been presented in some recent studies (Newinger and Burkhardt, 2012; Schumann and Graf, 2013) which demonstrated that daily air traffic density had an important impact on the contrail radiative forcing. However, it is worth noting that these two studies mainly focused on the diurnal cycle of contrail-cirrus radiative forcing, while illustrated in Fig.2 is for linear contrails.

Contrails induce a positive forcing due to longwave radiation coherent with the diurnal cycle in contrail ice mass with hourly emissions (Fig. 2c). The global longwave positive forcing is found to have a maximum of 12.5 mWm^{-2} at 1 PM local time and a minimum of 4.5 mWm^{-2} at 12 AM local time, with a diurnal average of 7.6 mWm^{-2}. However, when using daily or monthly averaged aircraft emissions, the longwave forcing shows little diurnal variation. This result seems to suggest that there is little daily variation in the aircraft emissions within each month. The diurnal average shows almost no variation when using hourly emissions (ensemble mean), daily or monthly emissions.

Contrails also produce a negative forcing due to shortwave radiation (Fig. 2b) with a stronger diurnal cycle. The largest negative forcing globally is found at 1 PM local time (-15.5 mWm^{-2} using the hourly emissions and -10 mWm^{-2} for daily or monthly emissions). A window with zero shortwave cooling is found between 8 PM and 4 AM local time, which is night time without solar radiation. The diurnal average in linear contrail shortwave forcing is -4.6, -3.6 and -3.6 mWm^{-2} using hourly, daily and monthly emissions, respectively.

The intensity of contrail shortwave forcing is regulated by the local solar zenith angle. When aircraft emissions are averaged on a daily or monthly basis, the number of daytime flights is reduced over regions where air traffic is mostly concentrated during the daytime, e.g. the Eastern US and Central Europe, and thus contrail formation during the daytime is decreased, underestimating shortwave forcing. The net effect of linear contrails (Fig. 2d) exhibits a strong diurnal cycle independent of the frequency of aircraft emissions due to the shortwave forcing. Even though the positive longwave forcing takes place around noon, it is mostly canceled out by the negative shortwave forcing. As a result, the net radiative forcing of linear contrails is peaked at both 7 AM and 7 PM (see Fig. 2d,h,l).

Our instantaneous calculations reveal that 113% of the contrail radiative forcing over the Eastern US is due to night flights (due to net negative forcing between 6 AM and 6 PM, Fig. 2), 66% of the contrail radiative forcing over Central Europe is due to night flights (Fig. 2l), and 92% of the global contrail radiative forcing is due to night flights (Fig. 2d). The portion of contrail radiative forcing due to night flights over the globe and over these two regions is higher than the global average attributed to night flights reported by Stuber and Forster (2007) (60%).

Due to the assumption on the life time of linear contrails in our first set of simulations, our estimated raditive forcing for linear contrails is likely to be lower than reality. First, linear contrails could persist longer than 30 minutes. Second, our experimental design would miss the lag effect reported in Newinger and Burkhardt (2012); Schumann and Graf (2013), i.e. the maximum in contrail coverage tends to lag the peak of air traffic density by a few hours.

3.2 *Monthly averaged contrail radiative forcing*

Both the instantaneous and integrated calculations exhibit a consistent seasonal cycle with higher positive radiative forcing during the Northern Hemisphere winter months (Fig. 3), which is consistent with atmospheric conditions in the UTLS more favorable for contrail formation and higher ice mass during the winter than in the summer (Chen et al., 2012).

In the instantaneous calculations, significant differences in the global radiative forcing are introduced when using hourly, daily, or monthly averaged aircraft emissions (Table 1). The simulation with hourly aircraft emissions produces the lowest radiative forcing throughout the year (Fig. 3a,b,c). Hourly aircraft emissions accurately represent the daily cycle of flights and capture the strong daytime negative shortwave forcing, thus resulting in weaker net radiative forcing.

The integrated effect of contrail cirrus is greater than the instantaneous effect. The monthly averaged forcing from the integrated calculation is roughly three times of that in the instantaneous calculations (Table 1). Because the integrated effects allow for longer contrail lifetimes, and water vapor emission impacts on natural cirrus, the integrated effect is less sensitive to the frequency of aircraft emissions input (hourly, daily, monthly, see Fig. 3d,e,f).

Table 1 has uncertainty reflecting meteorological variability. Uncertainties in contrail radiative forcing could be also induced by parametric assumptions made in our contrail initialization. For example, linear contrail radiative forcing increases by a factor of 9 when the particle diameter is reduced from 10 to 5 μm which almost scales linearly with the particle number concentration. The contrail radiative forcing decreases by a factor of 2.5 when the cross-sectional area is reduced to 100 m $\times$ 100 m. Based on Schröder et al. (2000), a diameter of 5 μm in particle size for young contrails (20-30 minutes) is too small. But a diameter of 7.5 μm can result in an increase in the particle number, and hence radiative forcing (scaling linearly with number concentration) by a factor of 2.5. Therefore, the uncertainty in Table 1 should be multiplied by a factor of 2.5 to account for the parametric uncertainty which is the uncertainty stated in the conclusion section. Additional uncertainties in contrail radiative forcing estimates could further result from the contrail particle shape.

The sensitivity of particle shape on the contrail radiative forcing has been investigated in several studies (Marquart et al., 2003; Rap et al., 2010; Markowicz and Witek, 2011) which suggested that the assumption of a spherical shape for contrail ice particles could result in a less intense shortwave forcing.

3.3 *Annual global and regional contrail radiative forcing*

A map of the radiative forcing based on the instantaneous calculations using hourly aircraft emissions (Fig. 4) indicates regions with substantial radiative forcing located along flight tracks over North America and Europe and the North Atlantic. Similar features are also found in the integrated effect as show in Fig. 5a,b. The global average radiative forcing at the top of the atmosphere under the instantaneous assumption simulated by CAM5-SD ranges from 2.9 to 4.5 mWm^{-2} (Table 1), depending on whether hourly, daily or monthly emissions are used. The forcing is 55% higher when using the monthly emissions compared with that using the hourly emissions. The net radiative forcing associated with contrail cirrus increases only 25% when using daily, instead of hourly, emissions (12.4 to 15.5 mWm^{-2} in Table 1). Therefore, the integrated effect of contrails is clearly much less sensitive to the daily cycle of flights than the instantaneous effect.

The global average may not be a good measure of the magnitude of contrail impact, especially within high air traffic corridors. The regional mean radiative forcing can reach 34 and 129 mWm^{-2} for Eastern US and Central Europe, respectively (boxes in Fig. 4b,c, as listed in Table 1 with hourly emissions). Similarly, even though contrail cirrus only produces a global forcing of 12.4 mWm^{-2}, the regional mean is roughly 200 and 600 mWm^{-2}, respectively. The local effect is as large as 400 mWm^{-2} (0.4 Wm-2) over much of the Northeastern US (Fig. 5c), and up to 1000 mWm^{-2} (1 Wm-2) over the highest air traffic regions of Western Europe (Fig. 5d).

The regional impact of contrail cirrus was also investigated in some recent studies. Burkhardt and Kärcher (2011) reported that radiative forcing of more than 300 mWm^{-2} could be induced by contrail cirrus over the Eastern US and Central Europe. Newinger and Burkhardt (2012) found that the contrail radiative forcing ranged between 100 and 300 mWm^{-2} over the US and between 200 and 500 mWm^{-2} over Western Europe (see their Fig. 3). These numbers are overall consistent with our simulations (see Table 1). However, Schumann and Graf (2013) reported a longwave radiative forcing of 720 mWm^{-2} over the North Atlantic area which is higher than our estimated longwave forcing over the Eastern US (630 mWm^{-2} using hourly emission, see Table 1) where air traffic density is even higher.

One important factor in controlling the uncertainties in contrail radiative forcing estimates is contrail optical depth (Stuber and Forster, 2007; Kärcher et al., 2010; Fromming et al. , 2011). In particular, Fromming et al. (2011) found nearly linear relationship between contrail radiative forcing and contrail optical depth. The ice water content and optical depth associated with contrail cirrus by the ensemble mean using hourly emissios can be seen in Fig. 6. The most pronounced simulated contrail optical depth is confined over the Eastern US and Central Europe, while the pertubation optical depth associated with contrail cirrus presented by Burkhardt and Kärcher (2011) was more wide spread with largest pertubations in the tropics. This explains why our estimate in contrail radiative forcing is lower than several previous studies.

4 Discussions and conclusions

Instantaneous calculations indicate that contrail radiative forcing is very sensitive to the frequency of aircraft emissions incorporated into CAM5-SD. Without the consideration of the daily cycle of flights, the simulations failed to capture the pronounced diurnal cycle of linear contrail formation and substantially reduced strong negative shortwave forcing in the afternoon hours leading to a 29% overestimate of contrail radiative forcing. Thus, it is essential to incorporate aircraft emission of high frequency into GCM simulations to produce credible assessments for linear contrail radiative forcing. Other factors which can strongly influence the estimate of linear contrail radiative forcing include the ice particle size, the cross-sectional area, and the lifetime of contrails.

The integrated contrail cirrus simulations, however, have lower sensitivity to the diurnal cycle of aircraft emissions. The overestimate by ignoring a diurnal cycle was only 25% for contrail cirrus. Consequently, using monthly averaged aircraft emissions in GCM simulations could produce reasonable integrated contrail radiative forcing but with a warm (high) bias to the estimates.

Contrail cirrus radiative forcing is roughly a factor of 4 larger than the effect of linear contrails. Assuming a linear relation between the forcing and the lifetime of contrails, the results imply that contrails last 2 hours on average which is reasonable compared with observations. The overall integrated effect of contrail cirrus by CAM5 is estimated 13±10 mWm^{-2} (from Table 1 with the multiplication of 2.5 to account for parametric uncertainty), lower than other recent estimates by Burkhardt and Kärcher (2011).

To put these results in perspective, contrail cirrus is a significant fraction of the global average aviation CO_2 radiative forcing of about 30 mWm^{-2} (Lee et al., 2010). It is also important to note that the 200-600 mWm^{-2} over Europe is a significant fraction of the total anthropogenic radiative forcing from long-lived greenhouse gases. Though the global effect of contrails is insignificant, the regional concentration of forcing might be important. One of the advantages of our method is that the contrail parameterization can be run inside

a full Earth System model with a coupled ocean to ascertain any effects on the surface temperature. The regional effect on the surface temperature is a subject of future investigation.

References

Appleman, H., 1953: The formation of exhaust condensation trails by jet aircraft. *Bull. Am. Meteorol. Soc.*, **34**, 14–20.

Barrett, S., et al., 2010: Guidance on the use of AEDT gridded aircraft emissions in atmospheric models, version 2.0, *Tech. rep.*, Federal Aviation Administration.

Burkhardt, U., B. Kärcher and U. Schumann, 2010: Global modeling of the contrail and contrail cirrus climate impact. *Bull. Amer. Meteor. Soc.*, pp. 479–483.

Burkhardt, U. and B. Kärcher, 2011: Global radiative forcing from contrail cirrus. *Nature*, **1**, doi:10.1038/NCLIMATE1068.

Chen, C.-C., A. Gettelman, C. Craig, P. Minnis and D. P. Duda, 2012: Global contrail coverage simulated by CAM5 with the inventory of 2006 global aircraft emissions. *J. Adv. Model. Earth Syst.*, **4**, doi:10.1029/2011MS000105.

Dietmüller, M. Ponater, R. Sausen and K.-P. Hoinka, 2011: Contrails, natural clouds, and diurnal temperature range. *J. Clim.*, **21**, 5061-5075, doi:10.1175/2008JCLI2255.1.

Frömming, C., M. Ponater, U. Burkhardt, A. Stenke, S. Pechtl, and R. Sausen, 2011: Sensitivity of contrail coverage and contrail radiative forcing to selected key parameters. *Atmos. Environ.*, **45**, 1483-1490.

Graf, K., U. Schumann, H. Mannstein and B. Mayer, 2012: Aviation induced diurnal North Atlantic cirrus cover cycle. *Geophys. Res. Lett.*, **39**, doi:10.1029/2012GL052590.

Gettelman, A., E. J. Fetzer, F. W. Irion and A. Eldering, 2006: The global distribution of supersaturation in the upper troposphere. *J. Climate*, **19**, 6089–6103.

Gettelman, A., X. Liu, S. J. Ghan, H. Morrison, S. Park, A. J. Conley, S. A. Klein, J. Boyle, D. L. Mitchell and J.-L. Li, 2010: Global simulations of ice nucleation and ice supersaturation with an improved cloud scheme in the Community Atmosphere Model. *J. Geophys. Res.*, **115**, D18216, doi:10.1029/2009JD013797.

Kärcher, B., U. Burkhardt, M. Ponater and C. Frömming, 2010: Importance of representing optical depth variability for estimates of global line-shaped contrail radiative forcing. *Proc. Natl. Acad. Sci. U.S.A.*, **107**(45), 19181-19184, doi:10.1073/pnas.1005555107.

Lee, D. S., D. W. Fahey, P. M. Forster, P. J. Newton, Ron C. N. Wit, Ling L. Lim, B. Owen and R. Sausen, 2009: Aviation and global climate change in the 21st century, *Atmos. Environ.*, **43**, 3520-3537.

Lee, D. S., G. Pitari, V. Grewe, K. Gierens, J. E. Penner, A. Petzold, M. J. Prather, U. Schumann, A. Bais, T. Bernsten, D. Iachetti, L. L. Lim and R. Sausen, 2010: Transport impacts on atmosphere and climate: Aviation. *Atmos. Env.*, **44**, 4678–4734.

Liu, X., R. C. Easter, Jr, S. J. Ghan, R. A. Zaveri, P. J. Rasch, X. Shi, J. F. Lamarque, A. Gettelman, H. Morrison, F. Vitt, A. Conley, S. Park, R. Neale, C. Hannay, A. M. Ekman, P. Hess, N. Mahowald, W. D. Collins, M. J. Iacono, C. S. Bretherton, M. G. Flanner and D. Mitchell, 2012: Toward a minimal representation of aerosols in climate models: description and evaluation in the Community Atmosphere Model CAM5. *Geosci. Model Dev.*, **5**(3), 709-739, doi:10.5194/gmd-5-709-2012

Markowicz, K. and M. Witek, 2011: Simulations of contrail optical properties and radiative forcing for various crystal shapes. *J. Climate*, **50**, 1740-1754, doi:10.1175/2011JAMC2618.1.

Marquart, S. and B. Mayer, 2002: Towards a reliable GCM estimation of contrail radiative forcing. *Geophys. Res. Lett.*, **29**, 1179, doi:10.1029/2001GL014075.

Narquart, S., M. Ponater, F. Mager and R. Sausen, 2003: Future development of contrail cover, optical depth and radiative forcing: impacts of increasing air traffic and climate change. *J. Climate*, **16**, 2890-2904.

Minnis, P., D. F. Young, D. P. Garber, L. Nguyen, W. L. J. Smith and R. Palikonda, 1998: Transformation of contrails into cirrus during SUCCESS. *Geophys. Res. Lett.*, **25**(8), 1157-1160.

Minnis, P., J. K. Ayers, R. Palikonda and D. Phan, 2004: Contrails, cirrus trends, and climate. *J. Clim.*, **17**, 1671-1685.

Morrison, H. and A. Gettelman, 2008: A new two-moment bulk stratiform cloud microphysics scheme in the Community Atmospheric Model (CAM3), Part I: description and numerical tests. *J. Climate*, **21**(15), 3642–3659.

Myhre, G. and F. Stordal, 2001: On the tradeoff of the solar and thermal infrared radiative impact of contrails. *Geophys. Res. Lett.*, **28**, 3119–3122.

Neale, R. B., C.-C. Chen, A. Gettelman, P. H. Lauritzen, S. Park, D. L. Williamson, A. J. Conley, R. Garcia, D. Kinnison, J.-F. Lamarque, D. Marsh, M. Mills, A. K. Smith, S. Tilmes, F. Vitt, H. Morrison, P. Cameron-Smith, W. D. Collins, M. J. Iacono, R. C. Easter, S. J. Ghan, X. Liu, P. J. Rasch and M. A. Taylor, 2010: Description of the NCAR Community Atmosphere Model (CAM 5.0). *NCAR Technical Note*, (http://www.cesm.ucar.edu/models/cesm1.0/cam/docs/description/cam5_desc.pdf).

Newinger, C. and U. Burkhardt, 2012: Sensitivity of contrail cirrus radiative forcing to air traffic scheduling *J. Geophys. Res.*, **117**, D10205, doi:10.1029/2011JD016736.

Rädel, G. and K. P. Shine, 2008: Radiative forcing by persistent contrails of its dependence on cruise altitude. *J. Geophys. Res.*, **113**, D07105, doi:10.1029/2007JD009117.

Rap, A., P. M. Forster, A. Jones, O. Boucher, J. M. haywood, N. Bellouin and R. R. De Leon, 2010: Parameterization of contrails in the UK Met Office Climate Model. *J. Geophys. Res.*, **115**, D10205, doi:10.1029/2009JD012443.

Schmidt, E., 1941: Die Entstehung von Eisnebel aus den Auspuffgasen von Flugmotoren. in Verlag R. Oldenbourg, editor, *Schriften der Deutschen Akademie der Luftfahrtforschung*, Vol. 44, pp. 1–15.

Schröder, F., B. Kärcher, C. Duroure, J. Strom, A. Petzold, J.-F. Gayet and B. Strauss, 2000: On the transition of contrails into cirrus clouds. *J. Atmos. Sci.*, **57**, 464–480.

Schumann, U. and P. Wendling, 1990: Determination of contrails from satellite data and observational results, *Proc. of a DLR*

Intern. Coll., Nov. 15/16, 1990, Lecture Notes in Engrg, **60**, Spinger-Verlag, Berlin, 138-153.

Schumann, U., 1996: On conditions for contrail formation from aircraft exhausts. *Meteorol. Z.*, **5**, 4–24.

Schumann, U., 2002: Contrail cirrus. in D. K. Lynch et al, editor, *Cirrus*, pp. 231–255. Oxford University Press.

Schumann, U. and K. Graf, 2013: Aviation-induced cirrus and radiation changes at diurnal timescales. *J. Geophys. Res.*, **118**, 2404-2421, doi:10.1002/jgrd.50184.

Stephens, G. L. and P. J. Webster, 1981: Clouds and climate: sensitivity of simple systems. *J. Atmos. Sci.*, **38**, 235–247.

Stordal, F., G. Myhre, E. J. G. Stordal, W. B. Rossow, D. S. Lee, D. W. Arlander, and T. Svendby, 2005: Is there a trend in cirrus cloud cover due to aircraft traffic? *Atmos. Chem. Phys.*, **5**, 2155-2162.

Stuber, N., P. Forster, G. Rädel and K. Shine, 2006: The importance of the diurnal and annual cycle of air traffic for contrail radiative forcing. *Nature*, **441**, 864-867, doi:10.1038/nature04877.

Stuber, N. and P. Forster, 2007: The impact of diurnal variations of air traffic on contrail radiative forcing. *Atmos. Chem. Phys.*, **7**, 3153-3162, odi:10.5194/acp-7-3153-2007.
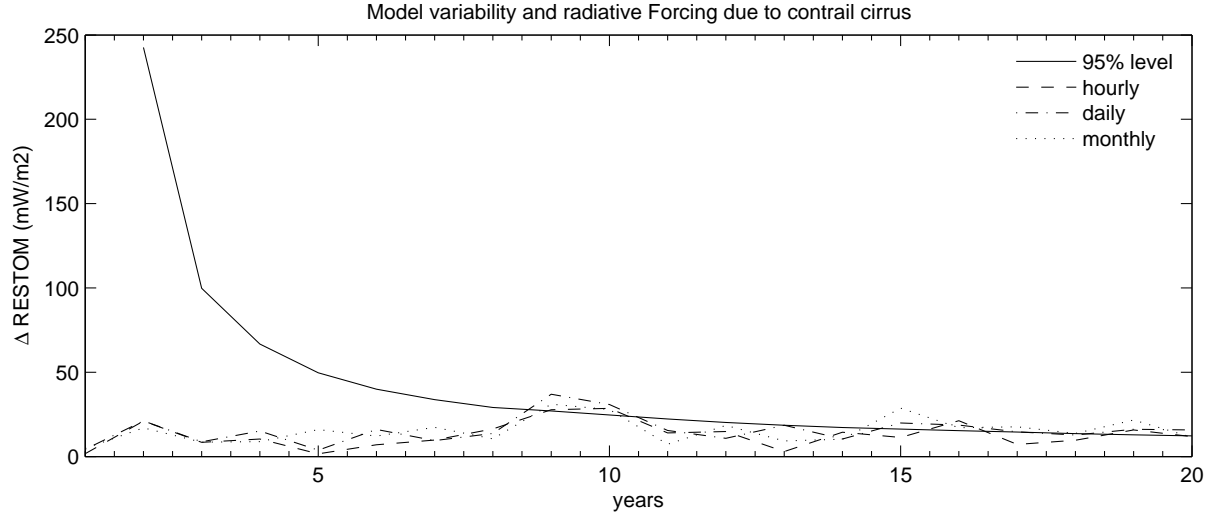
Fig. 1. Radiative forcing due to contrail cirrus: global annual averages using hourly (dashed line), daily (dash-dotted line), and monthly (dotted line) aircraft emission. Solid line is the significance threshold (95% confidence interval).

Table 1. Table of the global mean and regional averages over Eastern U.S. and Central Europe of shortwave radiative forcing at the top of the atmosphere (ΔFSNT), longwave radiative forcing at the top of the atmosphere (ΔFLNT), radiative forcing at the top of the atmosphere (Δ RESTOM), shortwave cloud forcing (Δ SWCF), longwave cloud forcing (ΔLWCF), and net cloud forcing (ΔCF) due to contrails and contrail cirrus from the instantaneous and integrated calculations by CAM5-SD simulations using hourly/daily/monthly aviation emissions. The uncertainty of the contrail radiative forcing from the simulations with hourly aviation emissions is represented by two standard deviations of the four ensemble members. All units in mWm^{-2}.

| Radiative forcing	Global	Eastern US	Central Europe
instantaneous ΔFSNT	-4.6±0.1/-3.6/-3.6	-91±5/-62/-62	-119±4/-84/-84
integrated ΔFSNT	-12.2±0.4/-19.3/-20.4	-430±42/-359/-348	-572±55/-430/-461
instantaneous ΔFLNT	7.6±0.2/7.6/7.6	118±5/117/117	227±14/209/209
integrated ΔFLNT	34±2/35/36	616±21/591/600	1130±127/1040/1043
instantaneous ΔRESTOM	3.1±0.2/4.0/4.0	26.7±5.0/55/55	108±12/125/125
integrated ΔRESTOM	12.4±4.0/15.7/15.5	185±30/232/252	577±81/610/583
instantaneous ΔSWCF	-4.6±0.1/-3.6/-3.6	-91±5/-62/-62	-119±4/-83/-84
integrated ΔSWCF	-21±5/-19/-20	-425±38/-356/-344	-567±58/-426/-452
instantaneous ΔLWCF	7.7±0.2/7.7/7.7	119±5/118/118	230±14/211/212
integrated ΔLWCF	37±2.2/39/40	630±22/607/615	1167±129/1082/1087
instantaneous ΔCF	3.1±0.2/3.6/3.6	28±5/56/56	111±12/128/127
integrated ΔCF	16±4/20/20	205±28/251/271	601±81/656/635
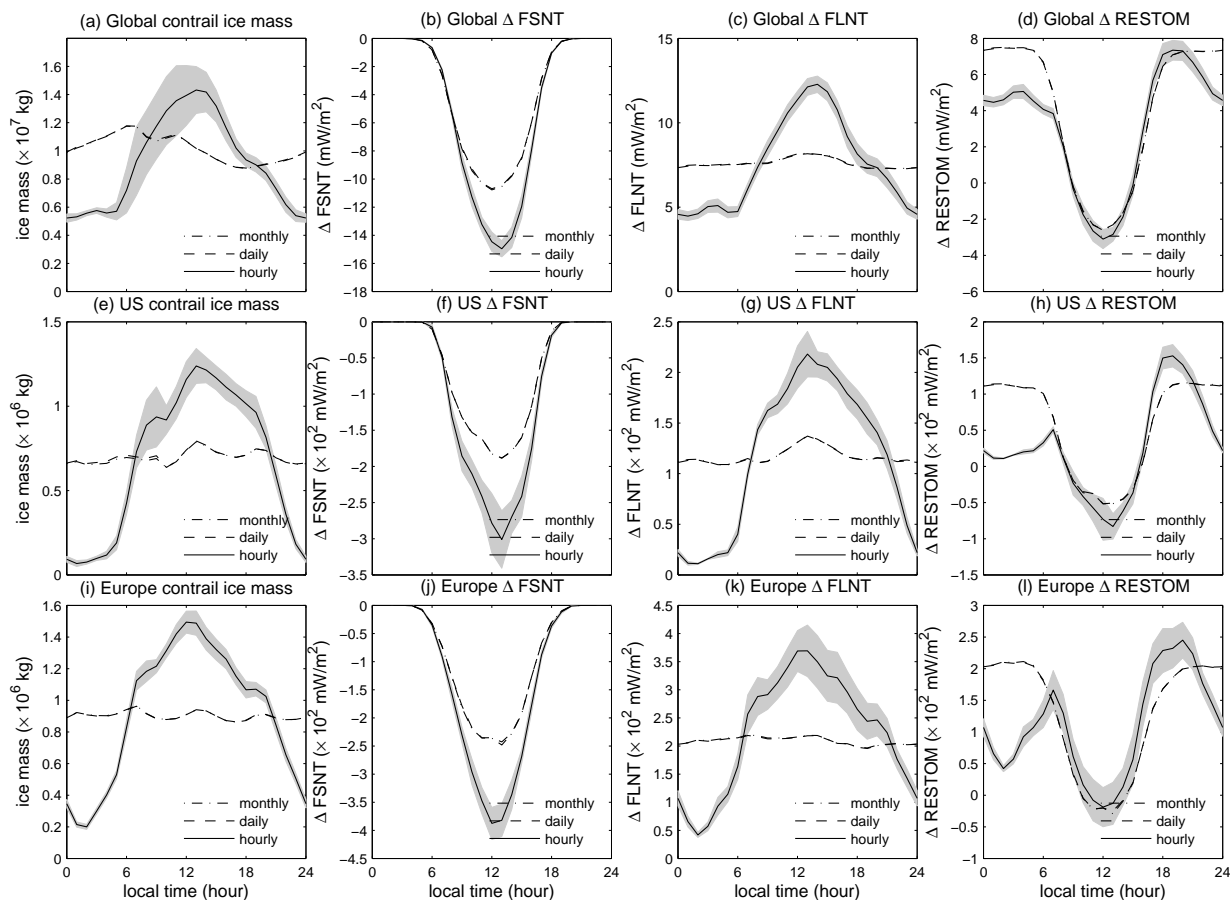
Fig. 2. The diurnal cycle of cloud ice mass, shortwave (FSNT), longwave (FLNT), and net radiative forcing (RESTOM) at the top of atmosphere based on diagnostic calculations by CAM5-SD with hourly, daily, and monthly averaged aircraft emissions over the globe, the Eastern US (denoted by the red box in Fig. 4b) and Central Europe (denoted by the red box in Fig. 4c) under the instantaneous assumption (linear contrails). The gray shading represents the ensemble mean $\pm$ two standard deviations using hourly aircraft emissions. The model output at each grid point is calibrated to its local time.
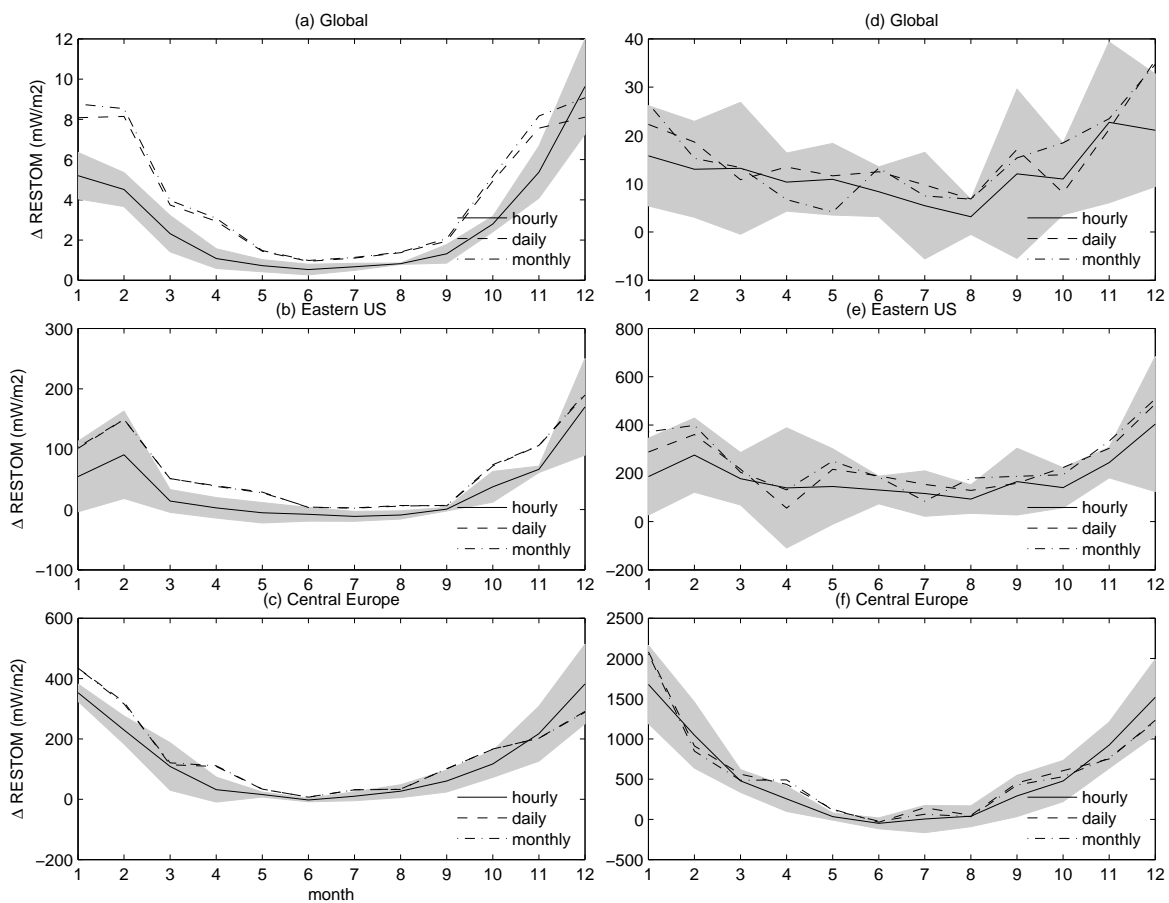
Fig. 3. The monthly averaged net radiative forcing over the globe, Eastern Us and Central Europe by CAM5-SD under instantaneous assumption (panels on the left) and the integrated calculations (panels on the right) with hourly, daily, and monthly averaged aircraft emissions, denoted by solid, dashed, and dashed-dotted lines. The gray shading represents the ensemble mean $\pm$ two standard deviations using hourly aircraft emissions. Note that the scale on each panel is different.
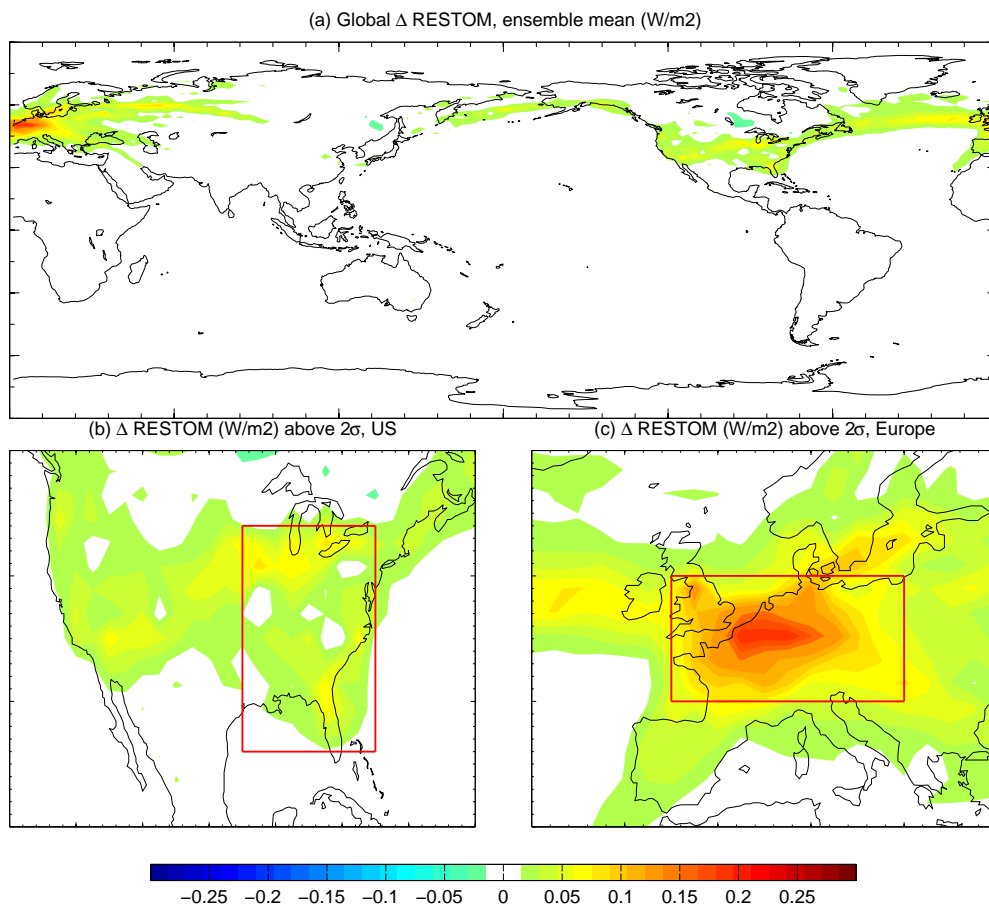
(a) Global Δ RESTOM, ensemble mean (W/m2)

(b) Δ RESTOM (W/m2) above 2σ, US

(c) Δ RESTOM (W/m2) above 2σ, Europe

−0.25 −0.2 −0.15 −0.1 −0.05 0 0.05 0.1 0.15 0.2 0.25

Fig. 4. The spatial distribution of net radiative forcing, in Wm^{-2}, at the top of the atmosphere based on instantaneous calculations by CAM5-SD with hourly averaged aircraft emissions. In (b) and (c), only the magnitude of perturbations in each grid cell that is above two standard deviations of the four ensemble members is plotted.
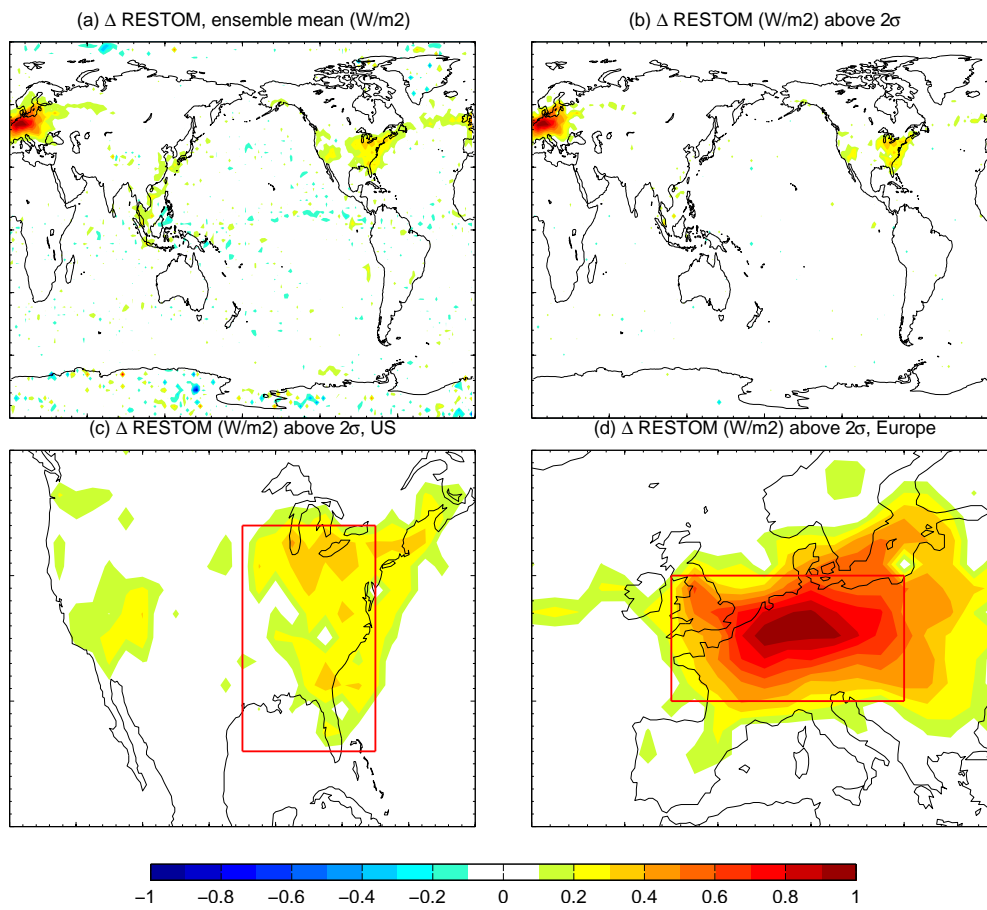
Fig. 5. Radiative forcing due to contrail cirrus: map of the ensemble mean by using hourly emissions in Wm^{-2}. (b) the magnitude of perturbations in each grid cell in (a) that is above two standard deviations of the four ensemble members.
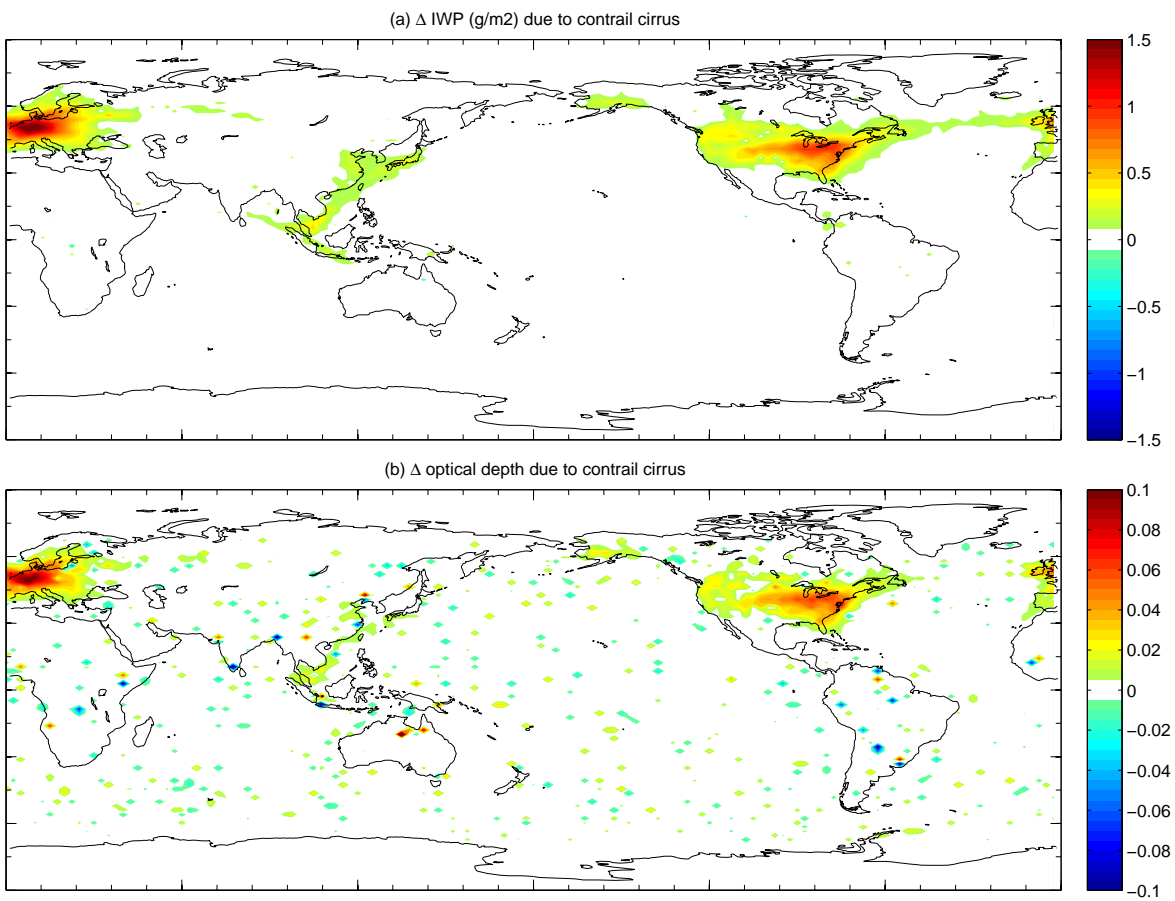
(a) Δ IWP (g/m2) due to contrail cirrus

(b) Δ optical depth due to contrail cirrus

Fig. 6. The spatial distribution of (a) ice water path in $\mathrm{gm^{-2}}$ and (b) optical depth due to contrail cirrus. The results are based on the ensemble mean of those simulations using hourly aircraft emissions and only pertubations above two standard deviations of the ensemble are plotted.